The geometry of the adsorbed complex was compared to that of the free species (Table 1). The methoxonium cation forms two strong hydrogen bonds, with nonbonded O–H distances as short as 1.35 Å. This value agrees with the trend observed in cluster calculations, in which the hydrogen bond length decreases as the size of the model increases; values as low as 1.41 Å have been observed for large systems. This finding is consistent with the behavior observed in $H_5O_2^+$, in which the proton almost symmetrically bridges between two water molecules with distances of close to 1.2 Å (*17*). The particularly strong hydrogen bonding also explains the large hydroxyl stretching frequency shifts observed in the infrared spectrum (*4*). Our calculated heat of adsorption for methanol, 82 kJ mol^{-1}, is within the large range of experimental estimates (63 to 120 kJ mol^{-1}) measured for various zeolites (*7*, *18*).

For comparison, we also examined the adsorption of methanol at an acid site in a highly siliceous form of the sodalite structure, again with a Si/Al ratio of 11. Although sodalite has the same number of atoms per unit cell as chabazite, the structure is very different, made up of β cages linked to give a small channel aperture, consisting of six-rings rather than the eight-rings found in chabazite. This structure does not have pores into which methanol could penetrate, and the acidic form is experimentally not known, but the sodalite cage is a unit found in several more complex structures such as zeolite A.

Steric hindrance prevents methanol from lying in the six-ring windows, and thus the molecule is situated in the more open cage region of the structure. We found that methanol was physisorbed instead of chemisorbed, with the proton remaining bound to the zeolite framework (Fig. 3). Despite the different structures of the adsorption complexes in the two structures, the binding energy of methanol in sodalite was similar to that in chabazite (73 kJ mol^{-1}).

We conclude that there is a delicate balance between the physisorbed and chemisorbed states of methanol in aluminosilicates. The nature of the adsorption complex is crucially dependent on the structure of the zeolite being considered. Contrary to previous cluster calculations (*6*, *7*), calculations taking into account the full periodicity of the zeolite structure show instances in which proton transfer from the zeolite to methanol takes place. In regions containing medium-sized pores, it appears that methanol is preferentially adsorbed and is activated through protonation. In the case of chabazite this process occurs in the eight-ring window, and we can infer from the catalytic activity of ZSM-5 that the same is probably true for 10-rings. When methanol is situated in the more open cage regions of zeolites, it appears to be unprotonated and potentially less chemically active.

We speculate that the medium-sized pores are the most active site for methanol reaction, because these are where methanol appears to be protonated. The presence of both methanol and methoxonium species in regions with different structural characteristics may explain the difficulty in unambiguously assigning experimental infrared spectra. We have demonstrated the potential of periodic ab initio calculations to treat molecular adsorption in aluminosilicates, which can now be extended to aid the elucidation of the reaction pathways of methanol within such heterogeneous catalysts.

Note added in proof: Our results for the case of adsorption of methanol in sodalite are consistent with recently published calculations of infrared spectra (*19*).

REFERENCES AND NOTES

1. J. M. Thomas, *Philos. Trans. R. Soc. London Ser. A* **333**, 173 (1990).
2. S. L. Meisel, J. P. McCullogh, C. H. Lechthaler, P. B. Weisz, *Chem. Technol.* **6**, 86 (1976).
3. M. W. Anderson and J. Klinowski, *Nature* **339**, 200 (1989).
4. G. Mirth, J. A. Lercher, M. W. Anderson, J. Klinowski, *J. Chem. Soc. Faraday Trans.* **86**, 3039 (1990).
5. G. Mirth and J. A. Lercher, in *Natural Gas Conversion*, A. Holmen *et al.*, Eds. (Elsevier, Amsterdam, 1991), pp. 437–443.
6. J. D. Gale, C. R. A. Catlow, J. R. Carruthers, *Chem. Phys. Lett.* **216**, 155 (1993).
7. F. Haase and J. Sauer, *J. Am. Chem. Soc.* **117**, 3780 (1995).
8. M. C. Payne, M. P. Teter, D. C. Allan, T. A. Arias, J. D. Joannopoulos, *Rev. Mod. Phys.* **64**, 1045 (1992).
9. P. Hohenberg and W. Kohn, *Phys. Rev.* **136**, B864 (1964); W. Kohn and L. J. Sham, *ibid.* **140**, A1133 (1965).
10. The Perdew-Wang functional was used [J. P. Perdew, in *Electronic Structure of Solids '91*, P. Zeische and H. Eschrig, Eds. (Akademie Verlag, Berlin, 1991).
11. A plane wave cutoff of 650 eV was used, and Brillouin zone sampling was performed only at the Γ point. We estimate the error due to these approximations to be about 2 kJ mol^{-1}.
12. Ab initio norm-conserving pseudopotentials were used. Those for carbon and oxygen were kinetic energy–optimized by Qc filter tuning [M. H. Lee *et al.*, in preparation.
13. Optimization was performed with no symmetry constraints, until forces were <0.03 eV/Å. The estimated error in energy of relaxed structure was <2 kJ mol^{-1}.
14. D. H. Aue and M. T. Bowers, in *Gas Phase Ion Chemistry*, M. T. Bowers, Ed. (Academic Press, New York, 1979), vol. 2, p. 18.
15. L. S. Dent and J. V. Smith, *Nature* **181**, 1794 (1958).
16. G. P. Tsintskaladze, A. R. Nefedova, Z. V. Gryaznova, G. V. Tsitsishvili, M. K. Charkviani, *Zh. Fiz. Khim.* **58**, 718 (1984).
17. Y. Xie, R. B. Remington, H. F. Schaefer III, *J. Chem. Phys.* **101**, 4878 (1994).
18. U. Messow, K. Quitzsch, H. Herden, *Zeolites* **4**, 255 (1984).
19. E. Nusterer, P. E. Blöchl, K. Schwarz, *Angew. Chem.* **35** (no. 2), 175 (1996).

20. This work was performed on the Cray T3D at Edinburgh Parallel Computing Centre as part of the United Kingdom Cas-Parinello and Materials Chemistry consortia. R.S. acknowledges the Engineering and Physical Sciences Research Council for financial support and J.D.G. thanks the Royal Society for provision of a University Research Fellowship.

27 October 1995; accepted 16 January 1996

Reversible Cleavage and Formation of the Dioxygen O–O Bond Within a Dicopper Complex

Jason A. Halfen, Samiran Mahapatra, Elizabeth C. Wilkinson, Susan Kaderli, Victor G. Young Jr., Lawrence Que Jr., Andreas D. Zuberbühler, William B. Tolman*

A key step in dioxygen evolution during photosynthesis is the oxidative generation of the O–O bond from water by a manganese cluster consisting of $M_2(\mu\text{–}O)_2$ units (where M is manganese). The reverse reaction, reductive cleavage of the dioxygen O–O bond, is performed at a variety of dicopper and di-iron active sites in enzymes that catalyze important organic oxidations. Both processes can be envisioned to involve the interconversion of dimetal-dioxygen adducts, $M_2(O_2)$, and isomers having $M_2(\mu\text{–}O)_2$ cores. The viability of this notion has been demonstrated by the identification of an equilibrium between synthetic complexes having $[Cu_2(\mu\text{–}\eta^2{:}\eta^2\text{–}O_2)]^{2+}$ and $[Cu_2(\mu\text{–}O)_2]^{2+}$ cores through kinetic, spectroscopic, and crystallographic studies.

Dioxygen O–O bond-forming and bond-cleaving reactions occur at transition metal centers in a number of enzymes. For example, O–O bond cleavage occurs at mononuclear heme (cytochrome P-450) (*1*) and nonheme di-iron (methane monooxygenase) (*2–4*) centers that hydroxylate alkanes to produce key metabolites. Similar reactions are needed for the oxidation of tyrosine by a dicopper active site to form L-dopa (tyrosinase) (*5*) and by a nonheme di-iron center to generate the catalytically essential radical of ribonucleotide reductase (*3*, *4*, *6*). The reverse reaction, the oxidative coupling of water molecules to form O_2

J. A. Halfen, S. Mahapatra, E. C. Wilkinson, V. G. Young Jr., L. Que Jr., W. B. Tolman, Department of Chemistry, University of Minnesota, Minneapolis, MN 55455, USA.
S. Kaderli and A. D. Zuberbühler, Institute of Inorganic Chemistry, University of Basel, CH-4056 Basel, Switzerland.

*To whom correspondence should be addressed.

in photosystem II, occurs at a tetranuclear Mn cluster that has been proposed to consist of two $Mn_2(\mu\text{–}O)_2$ components (structure **B**, M = Mn) (*4, 7*). Related Cu and Fe

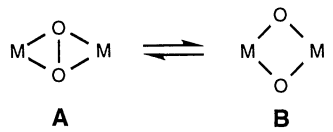

species with similar core structures that have recently been prepared have been found to be involved in biomimetic O_2 activation processes (*8, 9*). In addition, the existence of the isomeric $M_2(\mu\text{–}\eta^2{:}\eta^2\text{–}O_2)$ core structure (**A**) has been crystallographically established for M = Cu as exemplified by the structures of oxyhemocyanin (*10*) and a synthetic analog (*11*). The compositional similarity of these two structural motifs (**A** and **B**) suggests that a key step in O_2 activation at a dimetal center may be a transformation of **A** to **B** and that a pivotal

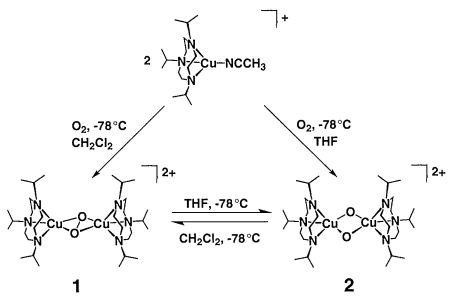

Fig. 1. Synthesis and interconversions of **1** and **2**.

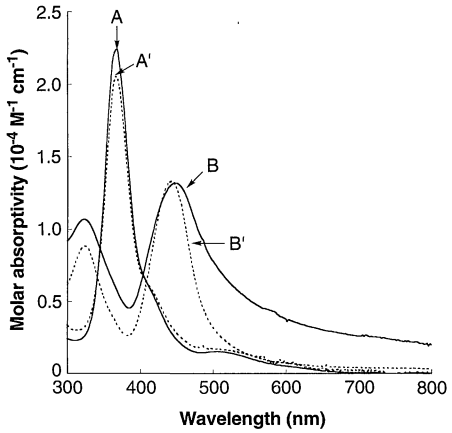

Fig. 2. Ultraviolet-visible spectra recorded at −80°C of (curve A) **1** in CH_2Cl_2 prepared by oxygenation of a CH_2Cl_2 solution of $[L^{iPr3}Cu(CH_3CN)]ClO_4$; (curve A′) **1** prepared by dilution of **2** (1.2×10^{-3} M) in THF with ~50-fold volume of CH_2Cl_2; (curve B) **2** in THF (turbid supension due to low solubility in pure THF, which results in the observed baseline absorption) prepared by oxygenation of a THF solution of $[L^{iPr3}Cu(CH_3CN)]ClO_4$; and (curve B′) **2** resulting from dilution of **1** (1.2×10^{-3} M) in CH_2Cl_2 with ~50-fold volume of THF.

step in O_2 evolution may simply be the reverse (*12*). We present here x-ray crystallographic support for structure **B** and demonstrate experimentally the interconversion between **A** and **B** for a synthetic system with M = Cu.

We recently reported (*13*) that oxygenation of the Cu(I) complex $[L^{iPr3}Cu(CH_3CN)](O_3SCF_3)$ (L^{iPr3} = 1,4,7-triisopropyl-1,4,7-triazacyclononane) in CH_2Cl_2 cleanly and reversibly produced an O_2 adduct (**1**, Fig. 1) with ultraviolet-visible (UV-vis) (curve A, Fig. 2) and Raman ($\nu_{O\text{–}O}$ = 722 cm^{-1}) features that are diagnostic of the $(\mu\text{–}\eta^2{:}\eta^2\text{-peroxo})$dicopper(II) core (*11, 14*). When the oxygenation of $[L^{iPr3}Cu(CH_3CN)](X)$ [X = PF_6^- or ClO_4^- (*15*)] was carried out in tetrahydrofuran (THF), a different species, **2**, was obtained quantitatively. This electron paramagnetic resonance (EPR)–silent molecule exhibits intense UV-vis features at 324 and 448 nm (curve B, Fig. 2) and a resonance Raman feature at 600 cm^{-1} that shifts to 580 cm^{-1} when prepared with $^{18}O_2$. These spectral properties are quite different from those of **1** but are nearly identical to those attributed to $[(L^{Bn3}Cu)_2(\mu\text{–}O)_2](ClO_4)_2$ (**3**), which was derived from the oxygenation of $[L^{Bn3}Cu(CH_3CN)]ClO_4$ (L^{Bn3} = 1,4,7-tribenzyl-1,4,7-triazacyclononane) in CH_2Cl_2 (Table 1) (*9*). We assign the UV-vis bands and the $^{18}O_2$-sensitive resonance Raman peak, respectively, to charge transfer transitions and a symmetric (A_{1g}) stretching vibration of the $\{Cu_2(\mu\text{-}O)_2\}^{2+}$ cores of **2** and **3**.

We have authenticated the structure of **3** by low-temperature x-ray crystallography (Fig. 3) (*16*). The $Cu_2(\mu\text{–}O)_2$ moiety is characterized by Cu···Cu [2.794(2) Å (numbers in parentheses represent errors in the last digit)], Cu–O (average = 1.81 Å), and O···O [2.287(5) Å] distances that are highly congruent with distances determined for other $M_2(\mu\text{–}O)_2$ (M = Fe, Mn) units (*7, 8*) but are distinct from those characteristic for the $Cu_2(\mu\text{–}\eta^2{:}\eta^2\text{–}O_2)$ core [for example, Cu···Cu = 3.560(3) Å, average Cu–O = 1.92 Å, and O–O = 1.41(1) Å for the complex reported in (*11*)]. The Cu···Cu and Cu–O distances in **3** are also significantly shorter than those typically found in bis(μ-hydroxo)dicopper(II) complexes (2.9 to 3.0 Å and 1.93 Å, respectively) (*17*), consistent with a higher overall oxidation level of the $Cu_2(\mu\text{–}O)_2$ core (*18*). The oxidizing capacity of both **2** and **3** is manifested in their common ability to activate aliphatic C–H bonds, as both compounds decompose upon warming through an oxidative N-dealkylation of their respective macrocyclic ligands that involves rate-determining ligand-substituent C–H bond cleavage (isopropyl methine C–H for **2**, benzylic C–H for **3**) (*19*).

The above results show that oxygen-

Table 1. Selected spectroscopic and physical properties of the $Cu_2\text{–}O_2$ adducts discussed in the text. All adducts exhibit 2:1 Cu:O_2 stoichiometry [**1–3**: low-temperature (−75°C) O_2 uptake manometry] and are EPR-silent; all other comments apply to the synthetic complexes alone. We measured the UV-vis spectra below −70°C using a custom-manufactured optical Dewar fitted with quartz windows (λ_{max}, wavelength of maximum absorption; ε, extinction coefficient). The resonance Raman spectra were obtained at −196°C as frozen solutions using 457-nm (**2** or **3**) or 514-nm (**1–3**) laser excitation or both; only ^{18}O-sensitive vibrations are quoted, with specific ^{18}O shifts in parentheses.

Core structure	Compound ligands (solvent)	UV-vis spectrum λ_{max} (nm)	UV-vis spectrum ε (M^{-1} cm^{-1})	Resonance Raman spectrum (cm^{-1})	Cu···Cu distance (Å)	Ref.
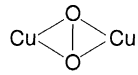	OxyHc 3 His/Cu (H_2O)	340 580	20,000 1,000	748 (708)	3.6(2) (x-ray)	(*10, 14*)
	1 L^{iPr3} (CH_2Cl_2)	366 510	22,500 1,300	722 (680)*		(*13*)
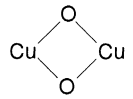	**2** L^{iPr3} (THF)	324 448	11,000 13,000	600 (580)		This work
	3 L^{Bn3} (CH_2Cl_2)	318 430	12,000 14,000	602–608† (583)	2.794(2) (x-ray)	(*9*), this work

*A weak vibration at 600 cm^{-1} (^{18}O at 580 cm^{-1}) was also observed with 514-nm excitation, indicative of the presence of a small percentage of **2**. †Occurs as a Fermi doublet that collapses to a single peak upon ^{18}O substitution.

ation of $[L^{iPr3}Cu(CH_3CN)]^+$ can produce either **1** or **2**, depending on solvent. More interestingly, **1** interconverts with **2** simply upon change of solvent (Figs. 1 and 2). Thus, addition of a solution of **1** in CH_2Cl_2 (2.4×10^{-3} M; curve A, Fig. 2) to a >10 fold excess volume of THF (all at −78°C) immediately yielded pure **2**, as shown by the dramatically changed optical spectrum (curve B′, Fig. 2) and the disappearance of ν_{O-O} in the resonance Raman spectrum (Table 1). The inverse addition of a solution of pure **2** in THF (curve B, Fig. 2) to a >10-fold excess of CH_2Cl_2 generated **1** (curve A′, Fig. 2). Mixtures of **1** and **2** were evident in solutions with intermediate solvent ratios. A ~4:1 mixture of **1** and **2** formed upon oxygenation of $[L^{iPr3}Cu(CH_3CN)]ClO_4$ in acetone at −78°C as indicated by the presence of features attributable to both species in UV-vis and resonance Raman spectra {peaks at 722 cm^{-1} [$\Delta\nu(^{18}O)$ = 42 cm^{-1}] and 602 cm^{-1} [$\Delta\nu(^{18}O)$ = 24 cm^{-1}]}, and this mixture could be accessed by addition of either **1** in CH_2Cl_2 or **2** in THF to excess acetone. The opposite dilution protocol (addition of the acetone mixture to CH_2Cl_2 or THF) also resulted in conversion into pure **1** or **2**, respectively. These combined experimental results show that the $[Cu_2(\mu\text{–}\eta^2{:}\eta^2\text{–}O_2)]^{2+}$ and $[Cu_2(\mu\text{–}O)_2]^{2+}$ cores can transmutate and suggest that **1** and **2** are in equilibrium, especially in solvents in which mixtures of the two compounds are apparent.

The existence of a rapid equilibrium between the two isomers was substantiated by the observed kinetics of the evolution and much slower decay of the mixture of **1** and **2** in acetone. Stopped-flow UV-vis monitoring of the formation of this mixture from the reaction of $[L^{iPr3}Cu(CH_3CN)]SbF_6$ with excess O_2 between −83° and −50°C revealed a clean first-order dependence on starting Cu complex concentration, no observable intermediate, and rate constants k for the generation of **1** and **2** that were identical to each other at each temperature (*20*) (Figs. 4 and 5). The decomposition rates of **1** and **2** were also the same (at −40°C, $k = 4.5 \times 10^{-3}\ s^{-1}$).

We explain these results by invoking an equilibrium between **1** and **2** that is established more rapidly than the initial O_2 binding step and the C–H bond cleavage governing their decomposition. Specifically, we propose that the oxygenation involves rate-determining formation of a mononuclear superoxo adduct (*21*, *22*) followed by faster trapping by a second monomeric Cu(I) starting complex and swift equilibration between **1** (which perhaps forms first) and **2**. The measured activation parameters $\Delta H\ddagger = 37.2 \pm 0.5$ kJ mol^{-1} and $\Delta S\ddagger = -62 \pm 2$ J K^{-1} mol^{-1}) are similar to those previously determined for the generation of the superoxo complex $[(BQPA)CuO_2]^+$ [BQPA = (bis-2-quinolyl)(2-pyridyl)methylamine] from a monocopper(I) precursor ($\Delta H\ddagger = 30 \pm 2$ kJ mol^{-1} and $\Delta S\ddagger = -53 \pm 8$ J K^{-1} mol^{-1}) (*22*), further supporting rate-determining superoxo-Cu complex formation in the reaction that ultimately yields **1** and **2**.

The experimental verification of the interconversion of $\{M_2(\mu\text{–}\eta^2{:}\eta^2\text{–}O_2)\}^{n+}$ (**A**) and $\{M_2(\mu\text{–}O)_2\}^{n+}$ (**B**) for M = Cu and n = 2 presented herein provides important precedence for the operation of analogous transformations in other synthetic and biological systems having M = Cu, Fe, or Mn (n = 2 or 4). Both the activation of O_2 through O–O bond splitting by metalloproteins and the evolution of O_2 involving O–O bond formation (*23*), as carried out by the Mn_4 cluster of photosystem II in plants, can be envisioned to proceed through the $[M_2(\mu\text{–}\eta^2{:}\eta^2\text{–}O_2)]^{n+} \rightleftharpoons [M_2(\mu\text{–}O)_2]^{n+}$ core isomerization. Our ability to directly observe this process for M = Cu attests to similar relative stabilities of the two cores supported by the L^{iPr3} macrocycle that are sensitive to solvent effects. The presence of features analogous to those we have assigned to the $Cu_2(\mu\text{–}O)_2$ core in spectra reported for other dioxygen-Cu adducts (*24*) further argues for the potential generality of the **A-B** interconversion. Definitive identification of the operation of this transformation in biological systems, as well as the more detailed characterization of this process in other synthetic compounds, should be investigated.

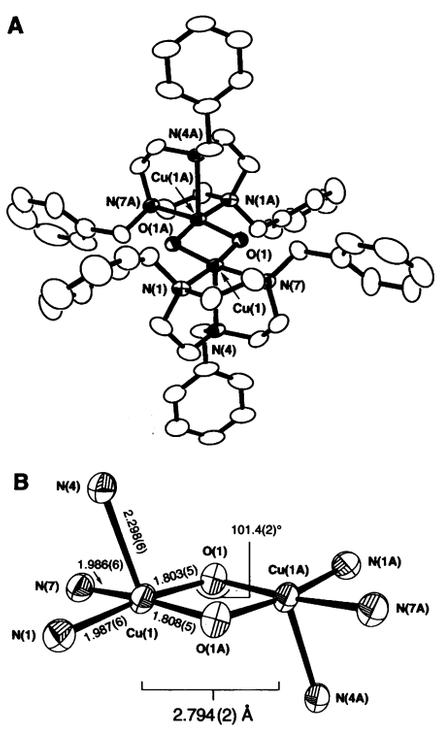

Fig. 3. (**A**) Representation of the low-temperature x-ray crystal structure of **3** shown with 35% thermal ellipsoids. Hydrogen atoms, SbF_6^- counterions, and solvent molecules are omitted for clarity. (**B**) View of the Cu coordination spheres (50% thermal ellipsoids) with relevant interatomic distances (in angstroms) and an angle noted.

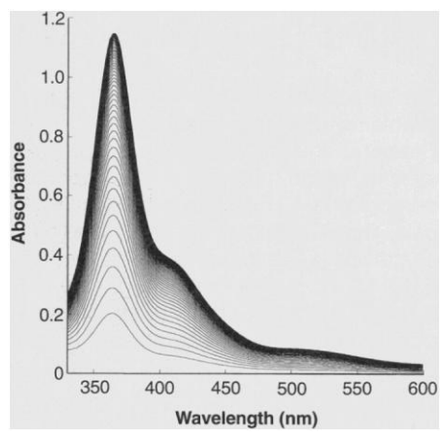

Fig. 4. Time-dependent (250 s, total) UV-vis spectra for the oxygenation reaction of $[L^{iPr3}Cu(CH_3CN)]SbF_6$ (6.3×10^{-4} M) to yield the mixture of **1** and **2** at −60°C; $[O_2] = 5.1 \times 10^{-3}$ M.

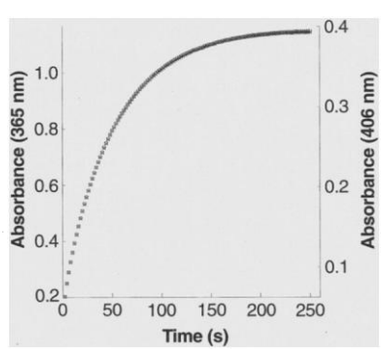

Fig. 5. Plots of absorbance versus time for the oxygenation reaction depicted in Fig. 4 at two wavelengths corresponding to **1** (365 nm; left y axis, ×) and **2** (406 nm; right y axis, ○). Identical rates of evolution of **1** and **2** are indicated by the congruence of the two plots [k(**1**) = k(**2**) = 1.77 $M^{-1}\ s^{-1}$].

REFERENCES AND NOTES

1. P. R. Ortiz de Montellano, *Cytochrome P-450: Structure, Mechanism, and Biochemistry* (Plenum, New York, 1986).
2. A. C. Rosenzweig, C. A. Frederick, S. J. Lippard, P. Nordlund, *Nature* **366**, 537 (1993); S.-K. Lee, B. G. Fox, W. A. Froland, J. D. Lipscomb, E. Münck, *J. Am. Chem. Soc.* **115**, 6450 (1993); S.-K. Lee, J. C. Nesheim, J. D. Lipscomb, *J. Biol. Chem.* **268**, 21569 (1993); K. E. Liu *et al.*, *J. Am. Chem. Soc.* **116**, 7465 (1994); K. E. Liu *et al.*, *ibid.* **117**, 4997 (1995).
3. A. L. Feig and S. J. Lippard, *Chem. Rev.* **94**, 759 (1994).
4. L. Que Jr. and A. E. True, *Prog. Inorg. Chem.* **38**, 97 (1990).
5. A. Sánchez-Ferrer, J. N. Rodríguez-López, F. García-Cánovas, F. García-Carmona, *Biochim. Biophys. Acta* **1247**, 1 (1995).
6. P. Nordlund, B.-M. Sjöberg, H. Eklund, *Nature* **345**, 593 (1990); P. Nordlund and H. Eklund, *J. Mol. Biol.* **232**, 123 (1993); J. M. Bollinger Jr. *et al.*, *J. Am. Chem. Soc.* **116**, 8024 (1994) and following papers in this issue.

7. K. Sauer, V. K. Yachandra, R. D. Britt, M. P. Klein, in *Manganese Redox Enzymes*, V. L. Pecoraro, Ed. (VCH, New York, 1992), pp. 141–175; V. K. Yachandra *et al.*, *Science* **260**, 675 (1993); K. Wieghardt, *Angew. Chem. Int. Ed. Engl.* **28**, 1153 (1989).
8. Y. Zang, Y. Dong, L. Que Jr., K. Kauffmann, E. Münck, *J. Am. Chem. Soc.* **117**, 1169 (1995); Y. Dong *et al.*, *ibid.*, p. 2778.
9. S. Mahapatra *et al.*, *ibid.*, p. 8865.
10. K. A. Magnus *et al.*, *Proteins: Struct. Funct. Genet.* **19**, 302 (1994).
11. N. Kitajima *et al.*, *J. Am. Chem. Soc.* **114**, 1277 (1992).
12. These ideas have been discussed; for example, see (*3*); V. L. Pecoraro, M. J. Baldwin, A. Gelasco, *Chem. Rev.* **94**, 807 (1994); D. M. Proserpio, R. Hoffmann, G. C. Dismukes, *J. Am. Chem. Soc.* **114**, 4374 (1992).
13. S. Mahapatra, J. A. Halfen, E. C. Wilkinson, L. Que Jr., W. B. Tolman, *J. Am. Chem. Soc.* **116**, 9785 (1994).
14. E. I. Solomon, M. J. Baldwin, M. D. Lowery, *Chem. Rev.* **92**, 521 (1992); E. I. Solomon, F. Tuczek, D. E. Root, C. A. Brown, *ibid.* **94**, 827 (1994).
15. The Cu(I) salts with these counterions produce the peroxo complex upon low-temperature reaction with O_2 in CH_2Cl_2.
16. Single crystals of **3** · $7(CH_3)_2CO \cdot 2CH_3CN$ were grown by oxygenation and subsequent storage of a solution of [d_{21}-$L^{Bn3}Cu(CH_3CN)]SbF_6$ (containing perdeuterated benzyl groups to slow decomposition) in 1:1 CH_2Cl_2:$(CH_3)_2CO$ at −78°C. We mounted a crystal on the side of a glass capillary at low temperature using a locally designed cold stage and transferred it to the goniometer of a Siemens SMART system, with the cryogenic stream set to −150°C for data collection. The structure was refined by full-matrix least squares on F^2 for all nonhydrogen atoms; hydrogen or deuterium atoms were included and refined by use of a riding model. The asymmetric unit contains one half of the dimeric cation as well as a CH_3CN and 3.5 $(CH_3)_2CO$ solvent molecules and a rotationally disordered SbF_6^- counterion. Distance restraints were placed on the solvent molecules, the SbF_6^- counterion, and the phenyl groups of the cation to force these units to conform to their respective average substructures. Crystal data **3** · 7 $(CH_3)_2CO \cdot 2\ CH_3CN$ ($C_{70}H_{72}D_{42}Cu_2F_{12}N_8O_9Sb_2$, molecular weight M_w = 1960.70): monoclinic space group *C2/c*, *a* = 26.1916(6) Å, *b* = 15.3560(4) Å, *c* = 22.2705(6) Å, β (crystallographic angle between *a* and *c*) = 96.493(1)°, cell volume *V* = 8899.7(4) Å^3, number of formula units per cell, *Z* = 8. Refinement of 523 variables based on 7863 reflections and 112 restraints converged at *R*1 = 0.1012 and weighted *R*2 = 0.2523 for data with reflection intensities $I > 2\sigma(I)$ using SHELXTL 5.0.
17. D. J. Hodgson, *Prog. Inorg. Chem.* **19**, 173 (1975); S. C. Lee and R. H. Holm, *Inorg. Chem.* **32**, 4745 (1993).
18. There are two possible resonance formulations of the $[Cu_2(\mu\text{–}O)_2]^{2+}$ core: bis(μ–oxo)dicopper(III) $[Cu^{III}_2(O^{2-})_2]^{2+}$ and bis(μ-oxyl)dicopper(II) $[Cu^{II}_2(O^{1-})_2]^{2+}$. Overall, the $[Cu_2(\mu\text{–}O)_2]^{2+}$ core is oxidized by two electrons compared to the $[Cu^{II}_2(OH)_2]^{2+}$ unit, which is produced upon its decomposition (*9, 19*). Experimental assignment of the Cu oxidation state in **2** and **3** is difficult on the basis of the available data; a molecular orbital picture of the bonding in their cores derived from ab initio calculations (*9*) that avoids formal charge assignments may be most appropriate.
19. A 3:2 mixture of unperturbed L^{iPr3} and 1,4-diisopropyl-1,4,7-triazacyclononane [R. P. Houser, J. A. Halfen, V. G. Young Jr., N. J. Blackburn, W. B. Tolman, *J. Am. Chem. Soc.* **117**, 10745 (1995)] (~90% overall yield) was identified by ^1H nuclear magnetic resonance spectroscopic and gas chromatographic–mass spectrometric analysis of the solution resulting from the warming of **2** in THF followed by treatment with aqueous NH_4OH. First-order rate constants for the decomposition of **2** and **2**-d_{42} (deuterated on the isopropyl substituents) in THF were obtained at temperatures between −58° and −10°C by UV-vis spectroscopic monitoring. Analysis using the Eyring equation yielded activation parameters ($\Delta H_H\ddagger$ = 55 ± 2 kJ mol^{-1}, $\Delta S_H\ddagger$ = −59 ± 8 J K^{-1} mol^{-1}, $\Delta H_D\ddagger$ = 64 ± 2 kJ mol^{-1}, $\Delta S_D\ddagger$ = −50 ± 8 J K^{-1} mol^{-1}) and kinetic isotope effects (KIE = k_H/k_D = 34 at −50°C; 11 at 25°C). The temperature dependence of the KIE is consistent with a tunneling contribution to the reaction rate, similar to that observed for the decomposition of **3** (*9*) and a previously reported peroxo-dicobalt complex [O. M. Reinaud and K. H. Theopold, *J. Am. Chem. Soc.* **116**, 6979 (1994)].
20. Two series of experiments with [[$L^{iPr3}Cu(CH_3CN)]SbF_6$] = 6.3 × 10^{-4} M, [O_2] = 5.1 × 10^{-3} M or [[$L^{iPr3}Cu(CH_3CN)]SbF_6$] = 1.73 × 10^{-3} M, [O_2] = 5.1 × 10^{-3} M were performed between −93° and +30°C. Of these we could successfully analyze a total of 30 runs in the range −82° and −50°C by assuming a simple second-order rate constant *k*, first order in [$L^{iPr3}Cu(CH_3CN)]^+$ and in O_2, followed by a fast irreversible step. At higher temperatures, incomplete adduct formation, secondary decay, and significantly changing spectra precluded simple numerical treatment. In all the kinetic experiments we used a modified SFL-21 low-temperature stopped flow unit (508 diodes, 1.3-ms minimum integration time, spectral range of 300 to 720 nm) and we analyzed the results using the program KINFIT. For further details, see (*22*).
21. K. D. Karlin, N. Wei, B. Jung, S. Kaderli, A. D. Zuberbühler, *J. Am. Chem. Soc.* **113**, 5868 (1991).
22. K. D. Karlin *et al.*, *ibid.* **115**, 9506 (1993).
23. Bimetallic catalysts for the oxidation of H_2O to O_2 have been reported: J. A. Gilbert *et al.*, *ibid.* **107**, 3855 (1985); D. Geselowitz and T. J. Meyer, *Inorg. Chem.* **29**, 3894 (1990); R. Ramaraj, A. Kira, M. Kaneko, *Angew. Chem., Int. Ed. Engl.* **25**, 825 (1986); Y. Naruta, M. Sasayama, T. Sasaki, *ibid.* **33**, 1839 (1994); M. Watkinson, A. Whiting, C. A. McAuliffe, *J. Chem. Soc. Chem. Commun.* **1994**, 2141 (1994).
24. For example, see: K. D. Karlin *et al.*, *J. Am. Chem. Soc.* **110**, 1196 (1988).
25. This research was supported by the Searle Scholars Program–Chicago Community Trust (W.B.T.), the Camille and Henry Dreyfus and Sloan Foundations (fellowships to W.B.T.), the National Science Foundation (National Young Investigator Award to W.B.T.), the National Institutes of Health (grant GM33162 to L.Q., grant GM47365 to W.B.T., and a predoctororal traineeship to E.C.W.), the University of Minnesota (Doctoral Dissertation Fellowship to J.A.H.), and the Swiss National Science Foundation (A.D.Z.).

11 October 1995; accepted 15 January 1996

High-Pressure Compounds in Methane-Hydrogen Mixtures

M. S. Somayazulu,* L. W. Finger, R. J. Hemley, H. K. Mao

The effect of pressure on chemical interactions in molecular mixtures is important for problems spanning fundamental chemistry, planetary science, and materials science. Diamond-anvil cell studies reveal pressure-induced chemistry in the CH_4-H_2 system. The system, which has no known compounds at ambient conditions, formed four molecular compounds, $CH_4(H_2)_2$, $(CH_4)_2H_2$, $CH_4(H_2)_4$, and CH_4H_2, at pressures up to 10 gigapascals. These have been characterized by synchrotron single-crystal x-ray diffraction, polycrystalline x-ray diffraction, Raman spectroscopy, and visual observation. Although $CH_4(H_2)_2$ crystallizes in the $MgZn_2$-type, hexagonal Laves phase structure, $(CH_4)H_2$ has a body-centered tetragonal structure that is similar to that of Al_2Cu. The 1:1 and 1:2 compounds are stable to at least 30 gigapascals.

Chemical interactions in dense materials are important in a broad range of problems in physical science, and the nature of such interactions in mixtures of simple molecular systems has become the focus of attention recently (*1*). Fundamentally, the study of such systems under pressure is important for theories of bonding in highly condensed states, for example, the evolution of bonding states (such as van der Waals, covalent, and metallic) with compression (*2*). Technologically, investigation of such systems, particularly those containing hydrogen, is important for the design of energetic compounds and hydrogen storage materials (*3*).

A wide range of pressures (up to several hundred giga-pascals) can be created with a diamond anvil cell. High-pressure studies have been conducted to explain how simple gases and liquids mix under pressure, and some early observations showed that mixtures of helium and nitrogen formed an unusual compound with the formula $He(N_2)_{11}$ under pressures of approximately 8 GPa. Chemical compounds that are stable only at high pressure were discovered (*4*) and termed van der Waals compounds (*5–7*). In addition, high-pressure H_2-H_2O (*8*) and He-H_2O (*9*) clathrates have been discovered. Here we present a detailed study of methane-hydrogen mixtures under pressure. The study revealed four new solid compounds having H_2:CH_4 molar ratios of 1:2, 2:1, 4:1, and 1:1.

A total of 17 different compositions in the CH_4-H_2 system were studied. The initial concentration of the mixture was fixed from the partial pressures of the gases, corrected with the virial coefficients. Each mixture was loaded in the diamond anvil cell after sufficient time for homogenization had been allowed (typically a week), with a ruby chip for pressure calibration. To minimize reaction of hydrogen, Be-Cu was used as the gasket material. For all our compositions, it was found that the

Geophysical Laboratory and Center for High Pressure Research, Carnegie Institution of Washington, 5251 Broad Branch Road, NW, Washington, DC, 20015 USA.

*On leave from the High Pressure Physics Division, Bhabha Atomic Research Center, Bombay 400 085, India.